VANCE PRESS

Rock Mechanics Letters

www.journal-rml.com

Research Article

Predicting horizontal principal stress through borehole deformation

Yunhong Wang[1,*]

[1] *Xi'an Research Institute of China Coal Technology&Engineering Group Corp,710077, China*
[*]Correspondence: w_202425@163.com

Received: 4 July 2025
Revised: 8 July 2025
Accepted: 8 July 2025
Published date: 30 July 2025
Doi: 10.70425/rml.202503.18

Abstract: In this paper, the geometry of borehole forced by two-dimensional stress was studied based on classical rock mechanics. The relation between horizontal principal stress and geometrical parameters of deformed circular borehole was established. The new prediction model of horizontal stress was deduced based on the above quantitative relation. Additionally, the stress computation was realized based on elliptical parameters of borehole. Subsequently, the feasibility and scientificity of the calculation method of horizontal principal stress were further confirmed via an experiment of borehole deformation based on borehole deformation. The feasibility and applicability of the method were verified based on actual drilling data in Xinjiang Province. The results demonstrated that the geometric shape of circular borehole after deformation was elliptical under the action of planar two-dimensional stress, and the horizontal principal stress could be expressed by the elliptic geometric parameters after deformation. The shape structure of the circular borehole under the action of non-uniform horizontal principal stress was elliptical, and the horizontal principal stress calculated using the parameters of the elliptical shape structure was directly proportional to the loading load. Larger the borehole diameter, smaller was the error of the method. The results provide new insights for in-situ measurement and inversion of deep horizontal in-situ stress.

Keywords: In-situ stress; borehole deformation; prediction; rock test; shape structure

1. Introduction

In-situ stress refers to the natural stress in strata without engineering disturbance. It is also known as initial stress of rock mass or primary rock stress [1-3]. As a key parameter in rock mass engineering, the fundamental force produces deformation and failure in mining and other underground engineering. With the increasing demand for economic development and resource exploitation, human beings have commenced deep engineering [4-5]. The depth of drilling in fields, such as hydropower, geothermal, mineral, and oil and gas, has attained thousands of meters. In deep engineering, high in-situ stress commonly exists, threatening the safety of engineering project construction. Accurate acquisition of deep in-situ stress is crucial for planning, design, and decision of engineering. In the field of coal mining, the size and direction of horizontal principal stress significantly impact the stability of the surrounding rock of the roadway [6]. In-situ stress measurement is a necessary prerequisite for determining the mechanical properties of engineering rock mass, analyzing the stability of surrounding rock mass, and completing the scientific excavation design of underground engineering. In the field of petroleum engineering, in-situ stress is a basic parameter for analyzing the stability of deep boreholes, studying the initiation and propagation of hydraulic fractures, predicting sand production, and preventing casing damage [7-9]. It is crucial for drilling, hydraulic fracturing, and gas production of deep oil gas.

In-situ stress measurement began during the 1930s. After nearly 100 years of technical development, mainly five method categories are present: borehole-based, core-based, geological, geophysical, and underground space-based [10-12]. The borehole-based method is the most direct technique for stress detection of deep rock mass. Most of the in-situ stress testing methods commonly used in engineering are also operated in boreholes. The method mainly applies the ellipticity or quasi-ellipticity of the borehole caused by stress concentration near the borehole after excavation and combines theoretical modeling to retrieve the in-situ stress. Regarding the issue of borehole deformation under the action of in-situ stress, researchers have extensively investigated theoretical derivation and measurement technology. Mukai et al. [13] developed a two-dimensional method for calculating principal stresses on a plane by measuring strain changes. Ziegler et al. [14]performed the diametrical core deformation analysis to determine the horizontal stress state. Another study examined the shear failure of borehole to indirectly calculate the principal stress. Kirsch et al. [15] proposed the Kirsch solution of rock stress and borehole deformation, which laid the theoretical foundation of the in-situ stress measurement method based on borehole deformation. A study derived the analytical solution of borehole wall displacement of circular borehole under far-field stress [16]. Another study analyzed borehole deformation under plane and three-dimensional stress states, and deduced the calculation formula of hole wall displacement under two stress states [17]. Zhang et al. [18] identified the analytical solution of displacement of deep buried circular roadway in transverse isotropic rock mass. Obert developed the Unites States Bureau of Mines (USBM) aperture deformation meter during the 1960s, which is the most representative aperture deformation measurement device with a round head piston, a cantilever beam, and a resistance strain gauge. Obara et al. [19] employed a laser displacement sensor to measure the displacement of borehole wall position and inverted the two-dimensional stress change of borehole plane by fitting elliptic function. In a study, researchers obtained the long- and short-axes of the ellipse after drilling deformation using the multi-arm caliper, and thereafter, retrieved the in-situ stress. Wang et al. [20] derived the formula of in-situ stress solution based on the shape parameters of the borehole and conducted the aperture deformation measurement experiment to verify the appropriateness of the formula of inversion of in-situ stress. A study used the contact-type aperture deformation monitoring instrument to measure the radial deformation at any three places of the borehole, and thereafter, inverted the size of the in-situ stress [21]. Although researchers have explored the inversion of in-situ stress based on borehole deformation, they have mainly focused on, laboratory verification and practical engineering are lacking.

The team of author has completed the numerical simulation on the borehole deformation under the horizontal principal stress [22]. Conclusively, it has not been deeply studied for establishing the prediction method of horizontal principal stress using the geometric parameters of elliptic borehole deformation. Therefore, the model of inversion of horizontal principal stress with borehole deformation was derived based on the relation between borehole deformation and in-situ stress under the condition of non-uniform horizontal principal stress. The appropriateness and feasibility of inversion of horizontal principal stress based on borehole deformation were verified via laboratory experiments. The feasibility of the method was further verified by applying it to practical engineering. The study promotes the extension of in-situ measurement and inversion methods of horizontal principal stress.

2. Derivation of the theoretical relation between horizontal stress and borehole deformation

2.1 Borehole deformation forced by horizontal stress

Fig. 1 illustrates the cross-section of the borehole. The circular borehole is pre-drilled in the formation with a radius of r. The formation is assumed to be infinite and media to be elastic, and the borehole is subjected to far-field stress. Additionally, the stress is assumed to be positive in the pull direction and negative in the pressure direction, and the coordinate axis coincides with the principal stress direction. In the x–y coordinate system, stress could be expressed as:

$$\{\sigma\} = \{\sigma_H, \sigma_h\} \tag{1}$$

where: σ_H is the maximum horizontal stress; σ_h is the maximum horizontal stress.

Based on the theory of elasticity, the radial displacement D_r and tangential displacement D_t of any point Q on the borehole are:

$$\begin{cases} D_r = -\dfrac{(1-v^2)r}{E}[(\sigma_H + \sigma_h) + 2(\sigma_H - \sigma_h)\cos 2\theta] \\ D_t = \dfrac{(1-v^2)r}{E}[2(\sigma_H - \sigma_h)\cos 2\theta] \end{cases} \tag{2}$$

where: E is The elastic modulus; v is Poisson's ratio; θ is the angle between the radial of the Q point and the positive x axis; r is the borehole radius.

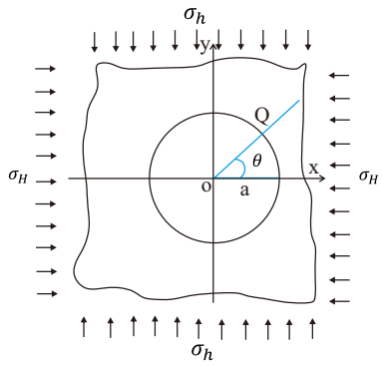

Fig. 1. Borehole displacement diagram

2.2 Elliptical structure of borehole forced by horizontal stress

Assuming that point Q is deformed to point Q', as shown in Fig. 2. Then, Eq. 3 could be achieved as follows.

$$\begin{cases} x = a \times \cos\theta + D_r \times \cos\theta - D_t \times \sin\theta \\ y = a \times \cos\theta + D_r \times \cos\theta + D_t \times \sin\theta \end{cases} \tag{3}$$

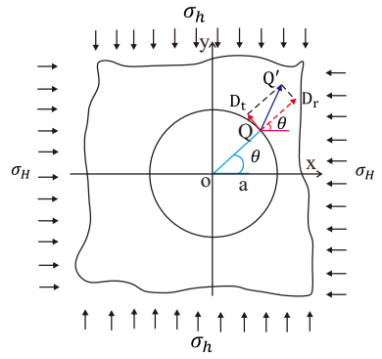

Fig. 2. Change of any point on the borehole wall

Substitute Eq. 2 into Eq.3; then Eq. 4 could be obtained after simplification.

$$\begin{cases} x = a[1 + (3\sigma_H - \sigma_h)/E]\cos\theta \\ y = a[1 + (3\sigma_h - \sigma_H)/E]\sin\theta \end{cases} \tag{4}$$

where

$$\begin{cases} A_0 = a[1 + (3\sigma_H - \sigma_h)/E] \\ B_0 = a[1 + (3\sigma_h - \sigma_H)/E] \end{cases} \tag{5}$$

Then Eq. 4 could be expressed as Eq. 6.

$$\begin{cases} x = A_0\cos\theta \\ y = B_0\sin\theta \end{cases} \tag{6}$$

Furthermore, Eq. 6 could be deduced as Eq. 7.

$$\begin{cases} \dfrac{x^2}{A_0^2} + \dfrac{y^2}{B_0^2} = \cos^2\theta + \sin^2\theta = 1 \end{cases} \tag{7}$$

That is the standard elliptic equation. However, because of the difference in the elastic modulus of rock at different depths, A_0 and B_0 vary with depth. Therefore, the geometric shape of circular borehole deformation under plane stress could be approximated as the ellipse. It has been theoretically established that the borehole shape structure forced by the stress is elliptical.

2.3 Prediction model based on the elliptical borehole deformation

Assuming that A and B are the lengths of the long and short semi-axes of an ellipse, respectively. When $A_0 > B_0$, then, $A = A_0$ and $B = B_0$, indicating the action of tension. When $B_0 < A_0$, then, $A = B_0$ and $B = A_0$, indicating the action of pressure. σ_H and σ_h could be expressed as Eq. 8.

$$\begin{cases} \sigma_H = \dfrac{3A_0 + B_0 - 4a}{8a} \\ \sigma_h = \dfrac{A_0 + 3B_0 - 4a}{8a} \end{cases} \tag{8}$$

For the elliptical borehole, the direction of the minimum horizontal principal stress is the direction of the long axis of the ellipse, and the long- and short-axes of the ellipse could be determined based on dual-diameter logging (Fig. 3). C13 and C24 correspond to the long- and short-axes of the elliptical borehole, respectively.

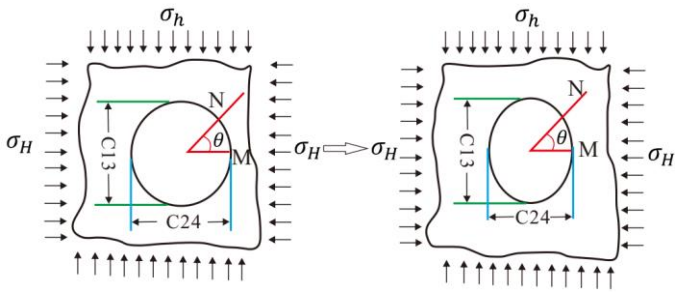

Fig. 3. Relation between the long- and short-axes of elliptic borehole and diameter

3. Borehole deformation experiments

3.1 Experiment instruments and rock samples

The experimental equipment for testing the mechanical properties of rock is RMT-150C mechanical testing machine developed by the Wuhan Institute of Rock and Soil Mechanics, Chinese Academy of Sciences. This equipment adopts digital control and electro-hydraulic servo, with high controllability, convenient operation, and high digital level. It is suitable for mechanical tests of rock and concrete materials, and could perform many kinds of rock mechanical tests, such as uniaxial compression, tensile, triaxial compression, and shear tests. The technical indicators of the equipment are presented in Table 1.

Table 1. Technical specifications of RMT-150 mechanical test machine

Technical index	Value
The maximum vertical output	1000.0kN
The maximum horizontal output	500.0kN
Vertical piston stroke	50.0mm
Horizontal piston stroke	50.0mm
The maximum confined pressure	50.0MPa
The rate of deformation	0.0001-1.0mm/s (13 level)
The rate of loading	0.001-100.0kN/s(13level)

The maximum axial force of the equipment is 1,000 kN and the maximum horizontal load is 500 kN, which can meet the requirements of the test. A unique advantage of the equipment is its capability to operate fatigue test under periodic load during the process of rock sample compression and direct shear. The RMT-150C mechanical testing machine

is depicted in Fig. 4. The rock samples are drawn from coal measure strata in Shaanxi—that is, sandstone, coal, and limestone, respectively (Fig. 5).

Fig. 4. Test equipment of drilling deformation. (a) RMT-150C rock-loading machine; (b) Camera used in the borehole

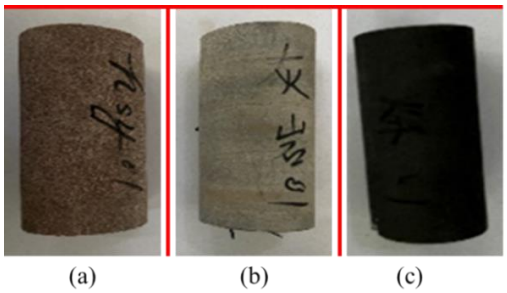

Fig. 5. Rock samples. (a) Sandstone; (b) Limestone; (c) Coal

3.2 Test process

To simulate the deformation of pre-borehole with different geometric sizes under different stress condition, the test comprises the following seven steps: (1) We made cube rock sample of size 150 mm×150 mm; (2) Subsequently, we drilled boreholes—according to experimental requirements, the diameter is set as four different values: 41 mm, 51 mm, 63 mm, and 74 mm (Fig. 6); (3) Thereafter strain gauge was stuck; (4) The confining pressure was set to conduct deformation experiment, and the confining pressure adopted displacement control; (5) High-precision camera was prepared to collect real-time deformation in the borehole; (6) Subsequently the experimental data were recorded; and (7) The deformation and damage of the borehole wall were analyzed. The RMT-150C rock mechanics test machine was used to conduct borehole deformation. The machine can complete both uniaxial compression and triaxial compression tests, meeting the requirements of this experiment. In the uniaxial loading test, the entire process of borehole wall was recorded and the dynamic process and failure form of borehole wall are captured. The change of the borehole structure during the loading process is a dynamic change process. It is the stage after the final rupture, that is, the ultimate stage after the three stages of initiation, stability, and rupture. These dynamically captured images help verify the deformation characteristics of the borehole structure.

It is a critical step to attach strain gauge on the borehole wall during the test. For this case, the strain gauge with small scale is selected, considering that the size of borehole is not large enough. The specific process of pasting is as follows: (1) Cleaning the borehole wall and drying it with cotton swabs dipped in alcohol; (2) Weld the strain gauge and wire; (3) Subsequently, a layer of epoxy resin glue is applied to the connection point and the back of the strain gauge for fixing; (4) Applying glue to the bottom of the strain gauge and sending it to the designated point in the borehole to paste; (5) Rolling back and forth on the surface of borehole with a small round rod to make it firmly paste on the borehole wall.

4. Results

4.1 Geometric structure of deformed borehole

Borehole deformation structure of rock samples with different lithologies and radius could be obtained by fitting the displacement data of the borehole wall collected by sensors. Under the action of maximum and minimum horizontal principal stresses, the standard circular boreholes tend to be elliptic deformation (Fig.s 7–9). Under the same borehole radius, the ellipticity of coal rock is greater than that of limestone (Fig.s 7–9). For the same lithology, the ellipticity of rock samples with radii of 51 mm and 63 mm is greater than that of rock samples with radius of 41 mm and 74 mm (Fig.s 7–9).

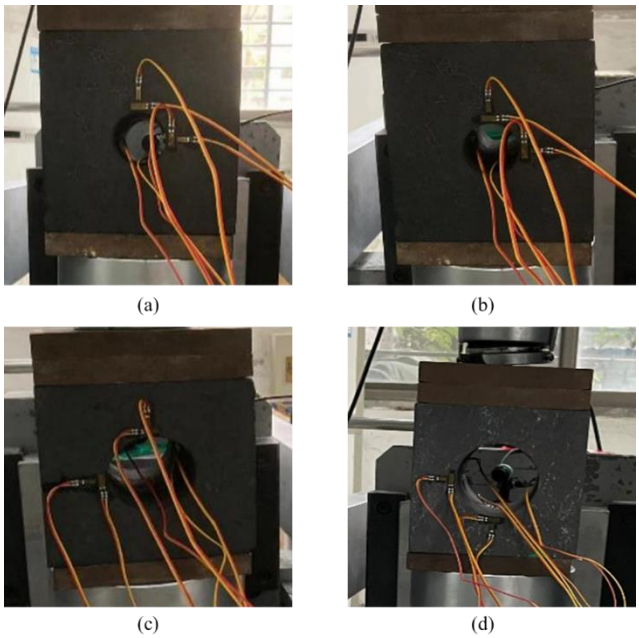

Fig. 6. Coal samples with pre-borehole. (a) r = 40 mm; (b) r = 51 mm; (c) r = 63 mm; (d) r = 74 mm

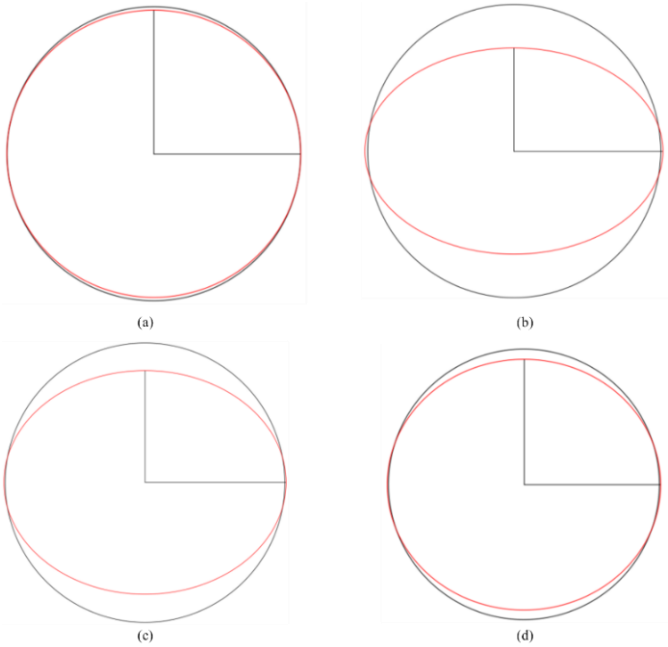

Fig. 7. Deformation track of borehole of coal. (a) Φ 40 mm; (b) Φ 51 mm; (c) Φ 63 mm; (d) Φ 74 mm

Overall, the deformation obtained *via* the experiment is consistent with that obtained *via* theoretical derivation. This confirms the elliptic mode of the borehole structure under the action of external load, indicating that this variation is somewhat related to horizontal stress. Stress load strength could be reflected in the deformation of the borehole structure. Therefore, from the perspectives of experiment and theory, the method of calculating horizontal principal stress by using borehole deformation under horizontal principal stress is logical and feasible. A set of systematic calculation methods and techniques of horizontal principal stress could be obtained.

For the radius of 40mm, being forced the condition of same horizontal principal stress, the ellipticity of sandstone is greater than that of coal and limestone. For the same lithology, the ellipticity of the radius of 51mm and 63mm is greater than that of 40mm and 74mm. It revealed that prediction model will has better effect in the sandstone formation than that of other

lithologies. The moderate radius of borehole is more conducive for the application of this method that of too large or small radius.

4.2 Comparison of prediction and test data

Based on the data recorded by the strains stuck on the borehole wall during loading, the data of strain gauge at different positions were converted into displacement data at different aperture directions using the transformation formula of strain and displacement of borehole wall. Based on the fitting results, the structure parameter values of the long and short semi-axes of the elliptic borehole under different loading conditions of each rock sample were obtained (Tables 2–4).

Principal stress values under different loading conditions were calculated using the prediction method of horizontal principal stress based on geometric parameters of elliptic borehole established in Section 2. During the loading, the confining pressure on the horizontal direction of the rock sample remained stable and fixed at 2 MPa. The load was gradually applied from the axial direction. The stress generated by the axial load was the maximum horizontal principal stress in the laboratory. Thereafter, the accuracy of the calculation method of horizontal principal stress, proposed in Section 2, was verified by comparing the calculated data with the test data. The horizontal principal stress calculated *via* the proposed method is presented in Table 5.

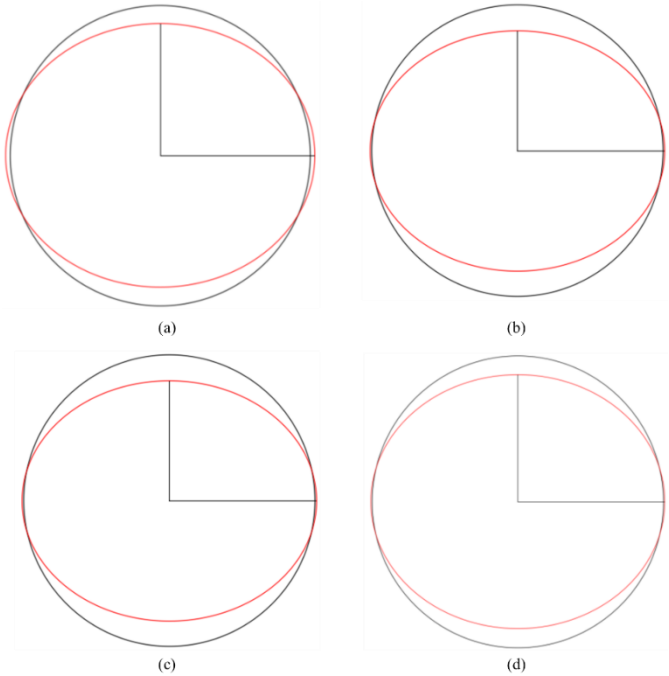

Fig. 8. Deformation track of borehole of sandstone. (a) Φ 40 mm; (b) Φ 51 mm; (c) Φ 63 mm; (d) Φ 74 mm

The calculated values were compared with the test values in the laboratory. The average errors between the calculated values and test values of different rock samples under different axial loads were ascertained. The comparison is presented in Fig. 10.

The calculated maximum principal stress values of coal, limestone, and sandstone under different loading conditions have several minor differences with the tested values, and the average error is less than 8%. The variation trend of the calculated values is consistent with that of the tested values, and the fluctuation range of the former is within the permissible error range of the actual project. The direction of the maximum principal stress is consistent with the loading direction, set as 0°. As indicated in Table 5, when the load is minor, a substantial gap is observed between the calculated and tested directions. With a gradual increase of load, the gap between the calculated and tested directions decreases. Thus, when the horizontal principal stress is minor—that is, less than 10 MPa—the horizontal principal stress will be less than 10 MPa. For this condition, it will generate substantial error when the direction of the principal stress is determined based on the proposed method. When the principal stress is major, the error of the direction of the maximum principal stress calculated *via* the proposed technique is less than the actual direction. Thus, it will have greater accuracy and is more scientific. Therefore, the proposed method is more suitable for determining the direction of the maximum principal stress in the high-stress region.

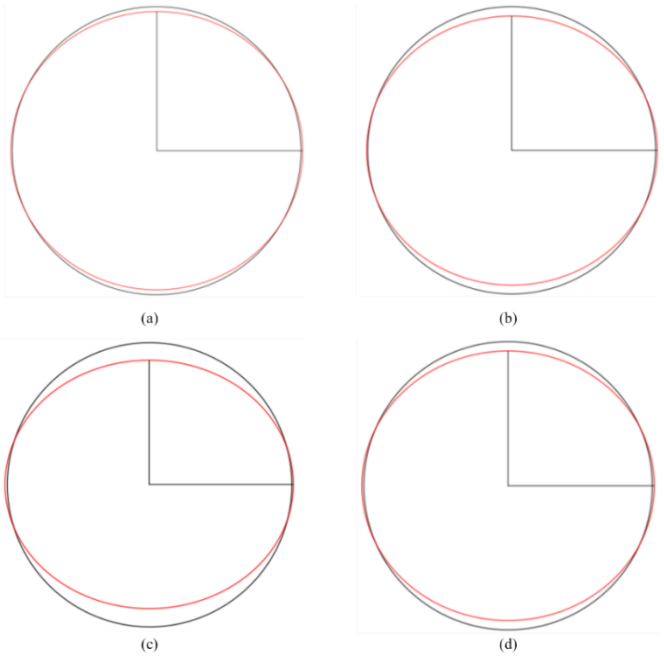

Fig. 9. Deformation track of borehole of limestone. (a) Φ 40 mm; (b) Φ 51 mm; (c) Φ 63 mm; (d) Φ 74 mm

In summary, the horizontal principal stress calculated via the proposed elliptic geometric parameter method could reflect the real stress condition of rocks. It is feasible, scientific, and accurate to a certain extent, and could be popularized and implemented in practical projects. For the high-stress environment, calculation of the principal stress direction using this method is more accurate.

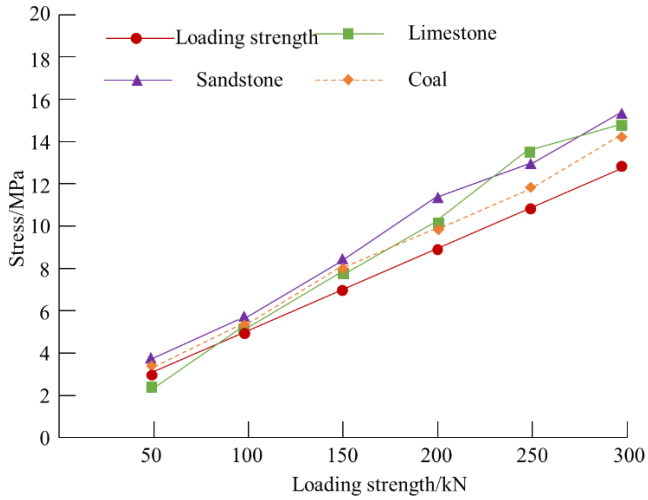

Fig. 10. Comparison of loading stress and maximum principal stress

5. Applied cases

Three drilling boreholes from Xinjiang were selected as applied cases of the proposed method (Fig. 11). The radii of the bit are 58, 89, and 130 mm. The three exploration boreholes were all core holes. The lithologies of the three holes are all limestone. The measured average Young's modulus were 36.7, 33.59, and 59.37 GPa, and Poisson's ratios were 0.281, 0.267, and 0.254. With the recorded aperture data at different depths, the maximum and minimum horizontal principal stress data were obtained using the method proposed in this study, as exhibited in Tables 7–8. The comparison between the predicted and tested data using the acoustic emission method revealed that the errors of the maximum and minimum horizontal principal stresses of the initial radius of 58 mm were 20.09 and 22.21 %, respectively. The errors of the initial aperture of 89 mm were 14.64 and 12.94 %. The errors of the initial radius of 130mm were 12.07 and 13.11 %. The average error of the direction of the maximum principal stress of the initial radius of 58 mm was 27.48 %, while the direction of

the calculated maximum principal stress was completely different from the measured direction for the initial radii of 89 and 130 mm, respectively.

The verification results of these three boreholes indicate that the smaller the initial radius, the larger the error of the calculated maximum and minimum horizontal principal stresses. The average relative error of the maximum and minimum horizontal principal stresses calculated by the borehole with the initial radii of 89 and 130 mm is less than 15%. Even though it has a certain error of 8% in the actual project, the absolute deviation fluctuates within the ± 5 MPa range. From the perspective of absolute deviation, the calculated horizontal principal stress could reflect the real characteristics of the *in-situ* stress of studied depth, and the calculated results are acceptable. The main reason for the substantial error is that the horizontal principal stress of the three boreholes is not large, and when the absolute deviation exceeds 3 MPa, the error will be higher. This necessitates the evaluation of prediction results by combining the absolute error, rather than the relative error. There is substantial difference between the calculated maximum principal stress direction and the measured ones because the method proposed in this study relied on the structural parameters of the elliptic borehole deformation being the action of horizontal principal stress. Actually, a certain gap remains between the fitted elliptic structure of deformed borehole and the actual morphology. As indicated by the actual cases in Xinjiang, when the stress of the surrounding rock of the borehole is low, this difference impacts the precision of the direction of the principal stress. Thus, it is advisable to apply the method proposed in this study to determine the direction of the principal stress, in combination with other methods to comprehensively evaluate the direction of the maximum principal stress.

Fig. 11. Actual borehole and core samples. (a)ZK001; (b)ZK002; (c) Core samples

Table 2. Borehole structure parameters of coal samples at different loading conditions

No.	Primary radius/mm	The loading strength/kN	The maximum principal stress/MPa	Long semi-axis/mm	Short semi-axis /mm
1	40	50	2.22	40.06028	39.96213
		100	4.44	40.11013	39.95864
		150	6.67	40.16286	39.94552
		200	8.89	40.22287	39.92438
		250	11.11	40.28014	39.89357
		300	13.33	40.34129	39.90627
2	51	50	2.22	51.09358	50.89759
		100	4.44	51.14193	50.85938
		150	6.67	51.22039	50.83965
		200	8.89	51.29158	50.80923
		250	11.11	51.36935	50.78731
		300	13.33	51.43856	50.75195
3	63	50	2.22	63.09258	62.97869
		100	4.44	63.18039	62.95025
		150	6.67	63.27118	62.91085
		200	8.89	63.36033	62.89356
		250	11.11	63.42779	62.86017
		300	13.33	63.53126	62.81735
4	74	50	2.22	74.11035	73.96194
		100	4.44	74.21153	73.93258
		150	6.67	74.32136	73.90018
		200	8.89	74.41675	73.86735
		250	11.11	74.51793	73.82854
		300	13.33	74.63052	73.79065

Table 3. Borehole structure parameters of sandstone samples at different loading conditions

No.	Primary radius/mm	The loading strength/kN	The maximum principal stress/MPa	Long semi-axis/mm	Short semi-axis /mm
1	40	50	2.22	40.02	39.96
		100	4.44	40.04	39.94
		150	6.67	40.05	39.92
		200	8.89	40.08	39.89
		250	11.11	40.10	39.87
		300	13.33	40.12	39.84
2	51	50	2.22	51.03	50.93
		100	4.44	51.05	50.91
		150	6.67	51.08	50.86
		200	8.89	51.10	50.85
		250	11.11	51.13	50.84
		300	13.33	51.15	50.83
3	63	50	2.22	63.04	62.92
		100	4.44	63.07	62.88
		150	6.67	63.10	62.83
		200	8.89	63.13	62.81
		250	11.11	63.16	62.79
		300	13.33	63.18	62.75
4	74	50	2.22	74.04	73.94
		100	4.44	74.08	73.88
		150	6.67	74.11	73.84
		200	8.89	74.15	73.80
		250	11.11	74.19	73.77
		300	13.33	74.22	73.74

Table 4. Borehole structure parameters of limestone samples at different loading conditions

No.	Primary radius/mm	The loading strength/kN	The maximum principal stress/MPa	Long semi-axis/mm	Short semi-axis /mm
1	40	50	2.22	40.00	39.98
		100	4.44	40.01	39.97
		150	6.67	40.02	39.95
		200	8.89	40.04	39.91
		250	11.11	40.06	39.90
		300	13.33	40.07	39.88
2	51	50	2.22	51.01	50.98
		100	4.44	51.01	50.97
		150	6.67	51.03	50.95
		200	8.89	51.05	50.92
		250	11.11	51.07	50.89
		300	13.33	51.09	50.83
3	63	50	2.22	63.01	62.98
		100	4.44	63.02	62.97
		150	6.67	63.03	62.95
		200	8.89	63.05	62.93
		250	11.11	63.06	62.91
		300	13.33	63.07	62.89
4	74	50	2.22	74.01	73.97
		100	4.44	74.02	73.96
		150	6.67	74.03	73.95
		200	8.89	74.05	73.94
		250	11.11	74.09	73.86
		300	13.33	74.11	73.81

Table 5. Comparison of loading stress value and calculation with borehole deformation structure method

No.	Primary radius/mm	The loading strength/kN	The tested maximum principal /MPa	The calculated maximum principal (Coal)/MPa	The calculated maximum principal (Sandstone)/MPa	The calculated maximum principal (Limestone)/MPa
1	40	50	2.22	2.13	2.01	2.11
		100	4.44	4.32	4.85	4.04
		150	6.67	6.48	6.74	5.92
		200	8.89	8.85	9.52	8.17
		250	11.11	10.96	12.59	13.22
		300	13.33	13.88	14.82	14.94
2	51	50	2.22	2.08	2.14	2.16
		100	4.44	3.35	3.86	4.18
		150	6.67	5.86	6.74	6.07
		200	8.89	8.02	8.68	9.31
		250	11.11	10.48	13.03	13.96
		300	13.33	12.51	15.69	14.95
3	63	50	2.22	2.43	2.35	2.34
		100	4.44	4.66	4.64	4.65
		150	6.67	6.87	6.35	7.27
		200	8.89	9.23	9.52	9.53
		250	11.11	10.84	12.53	11.75
		300	13.33	13.37	14.04	12.11
4	74	50	2.22	2.37	2.31	2.17
		100	4.44	4.57	4.56	4.26
		150	6.67	6.97	6.68	6.44
		200	8.89	9.01	9.34	8.76
		250	11.11	11.15	13.03	12.82
		300	13.33	13.57	15.13	14.12

Table 6. Calculation deviation of maximum principal stress direction (Let loading direction be the true direction of maximum principal stress)

Lithology	The loading strength/kN	The calculated direction of maximum principal stress/ °	Deviation
Coal	50	48.3625	48.3625
	100	21.1763	21.1763
	150	9.5729	9.5729
	200	4.6317	4.6317
	250	2.9254	2.9254
	300	2.0028	2.0028
Sandstone	50	49.0157	49.0157
	100	20.0293	20.0293
	150	9.2676	9.2676
	200	4.7653	4.7653
	250	2.8136	2.8136
	300	1.8598	1.8598
Limestone	50	49.1125	49.1125
	100	19.9368	19.9368
	150	9.1873	9.1873
	200	4.4275	4.4275
	250	2.3962	2.3962
	300	1.7259	1.7259

Table 7. Comparison between prediction and test values (Maximum horizontal principal stress)

No.	The radius of bit/mm	Depth/m	Long semi-axis/mm	Short semi-axis /mm	The maximum principal stress/MPa		
					Predicted values	Tested values	Deviation
		467.81	58.0986	57.9172	16.85	21.31	4.46
ZK001	58	483.56	58.1407	57.8685	22.95	29.18	6.23
		502.19	58.1575	57.8595	26.26	31.94	5.68
		619.37	89.1959	88.8182	19.15	23.02	3.87
ZK002	89	645.82	89.2262	88.7911	22.15	25.92	3.77
		667.21	89.2504	88.7614	24.17	27.64	3.47
		873.59	130.1021	129.9097	12.31	14.91	2.6
ZK003	130	891.32	130.1776	129.8499	21.85	23.58	1.73
		911.68	130.2191	129.81063	26.71	30.16	3.45

Table 8. Comparison between prediction and test values (Minimum horizontal principal stress)

No.	The radius of bit/mm	Depth/m	Long semi-axis/mm	Short semi-axis /mm	The maximum principal stress/MPa		
					Predicted values	Tested values	Deviation
		467.81	58.0986	57.9172	11.85	15.56	3.71
ZK001	58	483.56	58.1407	57.8685	20.19	26.73	6.54
		502.19	58.1575	57.8595	20.88	25.58	4.7
		619.37	89.1959	88.8182	16.49	21.13	4.64
ZK002	89	645.82	89.2262	88.7911	18.91	20.06	1.15
		667.21	89.2504	88.7614	21.97	24.71	2.74
		873.59	130.1021	129.9097	9.65	11.16	1.51
ZK003	130	891.32	130.1776	129.8499	15.57	18.54	2.97
		911.68	130.2191	129.81063	19.93	22.06	2.13

6. Discussion

6.1 Feasibility of the proposed method

Based on classical elastic mechanics, the was deduced that the shape of the deformed borehole under the non-uniform horizontal principal stress was elliptical. Furthermore, it was deduced that the maximum and minimum horizontal principal stresses were related to the long- and short-axes of the elliptical shape structure of deformed borehole. From the theoretical perspective, it was testified that the horizontal principal stress could be inversely calculated using the elliptic geometric parameters of the deformed borehole. This proved the feasibility of the theory of the proposed method. The experimental results of borehole deformation of sandstone, limestone, and coal confirmed the appropriateness of the theoretical derivation. The horizontal principal stress obtained using the tested data was positively correlated with the loading load. Despite some calculation errors, the variation trend is consistent—this further proves the feasibility of the method. For the practical application cases, the error between the calculated horizontal principal stress and the measured ones was less than 15%, which generally meets the error requirements of engineering. Thus, the method could be popularized and applied in practical engineering.

6.2 Impact factors of the proposed method

Addressing the constraints of drilling conditions is necessary to calculate horizontal principal stress using borehole deformation parameters. This will impact the accuracy of prediction and feasibility of implementation. The main impact factors include borehole radius, depth, and lithology. The applied cases indicated that the larger the borehole radius, the smaller the calculation error. This is mainly because the diameter deformation borehole with large diameter is greater than that of the borehole with small diameter under the same conditions. This method is more suitable for deep drilling. The *in-situ* stress value in deep rock mass is usually greater than that near the surface, and the borehole deformation forced by the *in-situ* stress is larger. Different lithologies may be encountered during deep drilling. The elastic modulus and Poisson's ratio of rocks are critical parameters to characterize the mechanical properties of rocks.

The difference between the elastic modulus and Poisson's ratio may lead to different stress distribution and transfer modes in the strata. It has a significant impact on the deformation and mechanical response of rocks. The errors of limestone and sandstone are smaller than that of coal, mainly because the rock strength of coal rock is less than that of limestone and sandstone. In the deep stratum, the formation stress is significant. The boreholes of coal can easily collapse and produce deformation, resulting in borehole collapse.

From the perspective of mechanism, it indicates that borehole deformation is mainly affected by two factors, namely, the physical chemical properties and the mechanical properties of the rock itself. These two factors are also manifested on the change of the mechanical properties of the rock. Thus, the physical and chemical properties are finally classified as mechanical properties. Presently, the obvious influence of physical and chemical properties on borehole deformation is soft mudstone and salt-paste rock. These two kinds of rocks are prone to creep when exposed to water due to the mineral components contained in them, which will also have certain effect on borehole deformation. However, carbonate and coal rock have weak expansion properties when exposed to water, and the influence on borehole deformation processing characteristics of these two kinds of rocks is almost negligible. The shape variables generated by physical and chemical properties can be ignored. The borehole deformation of coal and carbonate rock are all mechanical reasons.

6.3 The improvement of precision

Accurately determining the major and minor axes of the ellipse borehole is the primary key factor of the new method for prediction of horizontal principal stress. It indicates from the Eq.8 that the horizontal principal stress is related to the elastic modulus of rock, the long semi-axis A, short semi-axis B, as well as the initial borehole radius a. While the long semi-axis A and short semi-axis B can be measured in the field. Therefore, on the premise of ensuring the measurement accuracy, the main error of horizontal principal stress comes from the initial radius a of the borehole.

Assuming that the bit radius is a_z, the geometric property of ellipse borehole is determined by A and B. If the initial radius of the test borehole is set as the bit radius, that is, $a=a_z$, substituted into Eq.8, it can be obtained:

$$\begin{cases} x = a[1 + (3\sigma_H - \sigma_h)/E]\cos\theta \\ y = a[1 + (3\sigma_h - \sigma_H)/E]\sin\theta \end{cases} \tag{9}$$

$$\begin{cases} \sigma_H = \dfrac{3A + B - 4a_z}{8a_z}E \\ \sigma_h = \dfrac{A + 3B - 4a_z}{8a_z}E \end{cases} \tag{10}$$

Due to the error of actual borehole diameter, considering the relative diameter error τ, the bit radius is a^*, i.e.:

$$a^* = a_z(1 + \tau) \tag{11}$$

Substituting Eq.11 into Eq.8, it can be obtained:

$$\sigma_H^* = \frac{3A + B - 4a_z(1 + \tau)}{8a_z(1 + \tau)}E \tag{12}$$

$$\sigma_h^* = \frac{A + 3B - 4a_z(1 + \tau)}{8a_z(1 + \tau)}E \tag{13}$$

where σ_H^* and σ_h^* are the maximum and minimum principal stress calculated after considering the aperture error.

For the case of the maximum principal stress, the relative error τ_0 of stress calculation considering the relative error τ of diameter is:

$$\tau_0 = (\sigma_H^* - \sigma_h^*)/\sigma_H \tag{14}$$

After substituting σ_1, σ_1^* of Eq.9 and Eq.12 into Eq.14, it is simplified as following:

$$\tau_0 = \frac{1 + 4\tau a_z/(4a_z - 3B - A)}{1 + \tau} \tag{15}$$

After substituting Eq.11 into Eq.15, it can be simplified:

$$\tau_0 = \frac{1}{1+\tau} - 1 + \frac{1}{1+\tau}\left[\frac{4(a^* - a)}{3(a_z - B) + (a_z - A)}\right] \tag{16}$$

In Eq.16, (a^*-a_z) can be understood as the absolute diameter error generated during drilling, while 3(a_z-B)+(a_z-A) can be considered as the diameter deformation generated by force. The results show that the relative error τ_0 increases with the increase of diameter error within $\tau \ll 1$, but τ_0 decreases with the increase of borehole deformation. Meanwhile, it can be obtained from Eq.8:

$$3B + A - 4a_z = \frac{8\sigma_H a_z}{E} \tag{17}$$

By substituting Eq.17 into Eq.15, when τ_0 takes positive value, it can be obtained:

$$\tau_0 = \frac{-\tau}{1+\tau}\left(\frac{E}{2\sigma_H} + 1\right) \tag{18}$$

It can be seen from Eq.18 that the relation between the relative error τ_0 of the predicted stress and the principal stress is as follows: when the relative error τ of the borehole diameter remains unchanged, the greater the principal stress σ_H, the smaller the relative error τ_0 of the predicted stress; when the principal stress σ_H remains unchanged, the larger the relative error τ of the wellbore diameter, the larger the relative error τ_0 of the predicted stress. According to the above error analysis, certain applicable conditions and operating points in the process of in-situ stress testing based on wellbore deformation analysis exist as follows: (1) The quality of wellbore is strictly controlled, especially the wellbore diameter error; (2) New method is more suitable for wells with larger diameter, as the diameter deformation of wellbore with large diameter is larger than that with small wellbore diameter under the same conditions; (3) New method is more suitable for deeper drilling, as the in-situ stress in deep strata is usually larger than that near the surface, and the wellbore diameter deformation under in-situ stress is larger.

7. Conclusions

(1) It deduced the elliptical borehole shape, forced by the action of non-uniform horizontal stress, based on classical rock mechanics. It revealed that the maximum and minimum horizontal principal stresses could be reverse calculated using the morphological parameters of the ellipse.

(2) The experiment of borehole deformation further proves that the standard circular borehole presents elliptic deformation mode under the non-uniform horizontal principal stress. The elliptic deformation is related to lithology, rock mechanical parameters, and borehole size.

(3) The horizontal principal stress calculated in the laboratory with the proposed method is positively correlated with the loading stress, confirming the feasibility of the method based on borehole deformation parameters. The actual applied cases indicate that the larger the radius, the smaller the error of the proposed new method in predicting horizontal principal stress. The proposed method is more suitable for borehole point at greater depth and radius.

Author contributions

Yunhong Wang completed all work.

Acknowledgements

Funding was provided by the Research on multi-field and multi-attribute dynamic analysis technology of geological hazards (grant No. 2023YFC3008903-05), General research project of Zhejiang Provincial Department of Education (Y202456528)

Conflict of interest statement

On behalf of all authors, the author states that there are no conflicts of interest.

Data availability

The datasets generated and analysed during the present study are not publicly available because of applicable institutional guidelines but are available from the corresponding author upon reasonable request.

References

1. Fang XX, Feng H. An improved method for predicting horizontal principal stress: A Case involving a P Gas Field in Northeastern Sichuan. Geotechnical and Geological Engineering. 2023; 41: 1137-1154. https://doi.org/10.1007/s10706-022-02327-y.
2. Fang XX, Feng H. In situ stress characteristics of the NE Sichuan basin based on acoustic emission test and imaging logging. SN Applied Sciences. 2021; 12: 871-883. https://doi.org/10.1007/s42452-021-04836-6.
3. Kang HP, Lin J, Zhang X. Research and application of in-situ stress measurement in deep mines. Chinese Journal of Rock Mechanics and Engineering. 2007; 26: 929-934.
4. Chang C, Li S, Tang DZ. In-situ stress calculation for coal reservoirs based on log parameters: A case study of the southern Yanchuan block. Coal Geology& Exploration. 2023; 51: 23-32. https://doi.org/10.12363/issn.1001-1986.22.09.0726.
5. Meng ZP, Tian YD, Li GF. Characteristics of in-situ stress field in southern Qinshui Basin and its research significance. Journal of China Coal Society. 2010; 35: 975-981. https://doi.org/10.13225/j.cnki.jccs.2010.06.014.
6. Zhao HF, Yang CZ, Feng K. Inversion analysis of three-dimensional geostress field in northwest Hancheng Block. Safety in Coal Mines. 2023; 54: 16-23. https://doi.org/10.13347/j.cnki.mkaq.2023.10.003.
7. Sang SX, Zheng SJ, Wang JG. Application of new rock mechanical stratigraphy in sweet spot prediction for deep coalbed methane exploration and development. Acta Petrolei Sinica. 2023; 44: 1840-1853.
8. Xie ZL, Liu ZD, Han H. Log-based in situ stress prediction of deep coalbed methane reservoirs in the Daji block. Geophysical & Geochemical Exploration. 2024; 48: 356-365. http://doi.org/10.11720/wtyht.2024.2600.
9. Cao H, Zhao Y, Shuai D. Using 3D seismic data to estimate stress based on seismic curvature attribute of HTI medium. Chinese Journal of Geophysics. 2024; 67: 1970-1986. http://doi.org/10.6038/cjg2023Q0791.
10. Tan NG, Yang RS, Tan ZY. In-situ stress measurement while drilling and stress characteristics at the margin of Ordos Plateau. Chinese Journal of Engineering. 2024; 46: 581-588. http://doi.org/10.13374/j.issn2095-9389.2023.06.07.001.
11. Wang B, Qin XH, Chen QC. Measurement results of in-situ stress in Guyuan area of Ningxia on the southwest margin of Ordors block and its causation analysis. Geological Bulletin China 2020; 39: 983-993.
12. Zhu MD, Wang ZY, Zhang YZ. In-situ stress measurement and inversion analysis of the deep shaft project area in Sanshan Island on hydraulic fracturing method. Journal of Geomechanics. 2023; 29: 430-441. http://doi.org/10.12090/j.issn.1006-6616.20232911.
13. Mukai A, Yamauchi T, Hiroshi I. In situ stress measurement by the stress relief technique using a multi-component borehole instrument. Earth Planets Space. 2007; 59: 133-139.
14. Bahrehdar M, Lakirouhani A. Assessment of interplay of mud cake and failure criteria on the lower limit of safe borehole pressure. Indian Geotechnique Journal. 2023; 7: 1-13. https://doi.org/10.1007/s40098-023-00856-8.
15. Kirsch G. Die theorie der elastizitat und die bedurfnisse der festigkeitslehre. Veit Ver Deut Ing. 1898; 42: 797-807.
16. Jaeger CJ, Neville GWC. Fundamentals of rock mechanics. 2009; UK: John Wiley & Sons..
17. Wang LJ. Crustal stress measurements and their application in engineering. Beijing: Geological Publishing House. 1991; 1-31.
18. Zhang ZZ, Li ZK, Xu MG. Displacement analytic solution of deep buried circular tunnel in transverse isotropy rock mass. Gold. 2010; 31: 23-26.
19. Obara Y, Shin T, Yoshinaga T. Cross-sectional borehole deformation method (CBDM) for measurement of rock stress change. 5th International Symposium on In-Situ Rock Stress. 2010; 129-134.
20. Wang CY, Han ZQ, Wang JC. Study of borehole geometric shape features under plane stress state. Chinese Journal of Rock Mechanics and Engineering. 2016; 35: 2836-2842. https://doi.org/10.13722/j.cnki.jrme.2015.1045.
21. Wang CY, Wang YT, Han ZQ. An in-situ stress measurement method based on borehole shape analysis. Rock and Soil Mechanics. 2019; 40: 549-557. https://doi.org/10.16285/j.rsm.2018.1926.
22. Fang XX, Ma SJ, Wang YH. Experimental and numerical simulation investigation of the deformation characteristics of vertical boreholes under non-uniform horizontal principal stress. Geomechanics and Geophysics for Geo-energy and Geo-resources. 2024; 10: 1-25. https://doi.org/10.1007/s40948-024-00799-1.